Evolution of Bloch-mode envelopes in two-dimensional generalized honeycomb lattices

Mark J. Ablowitz and Yi Zhu*

Department of Applied Mathematics, University of Colorado, 526 UCB, Boulder, Colorado 80309-0526, USA

(Received 20 May 2010; published 30 July 2010)

Wave propagation in two-dimensional generalized honeycomb lattices is studied. By employing the tight-binding (TB) approximation, the linear dispersion relation and associated discrete envelope equations are derived for the lowest band. In the TB limit, the Bloch modes are localized at the minima of the potential wells and can analytically be constructed in terms of local orbitals. Bloch-mode relations are converted into integrals over orbitals. With this methodology, the linear dispersion relation is derived analytically in the TB limit. The nonlinear envelope dynamics are found to be governed by a unified nonlinear discrete wave system. The lowest Bloch band has two branches that touch at the Dirac points. In the neighborhood of these points, the unified system leads to a coupled nonlinear discrete Dirac system. In the continuous limit, the leading-order evolution is governed by a continuous nonlinear Dirac system. This system exhibits conical diffraction, a phenomenon observed in experiments. Coupled nonlinear Dirac systems are also obtained. Away from the Dirac points, the continuous limit of the discrete equation leads to coupled nonlinear Schrödinger equations when the underlying group velocities are nearly zero. With semiclassical approximations, all the parameters are estimated analytically.

DOI: 10.1103/PhysRevA.82.013840 PACS number(s): 42.65.Tg, 05.45.Yv, 42.81.Dp

I. INTRODUCTION

Wave propagation in nonlinear periodic media is of keen interest and has resulted in new and interesting phenomena [1–5]. These studies have been stimulated by rapid experimental advances in optics, Bose-Einstein condensates (BEC), and related fields. In optics, high-intensity laser beams that propagate in periodic structures, such as periodic wave-guide arrays and photonic lattices, naturally combine periodicity and nonlinearity [2,3]. In BEC, condensates are loaded into periodic optical lattices in addition to a harmonic trap. The existence of the periodic optical lattices leads to rich and complex condensate patterns [5]. The problems mentioned previously in the two fields (optics and BEC) are closely related, since their mathematical descriptions are similar.

Localized structures that propagate without change of shape have a potential application for information-light switching and optical information. Many novel localized structures, referred to as solitons, have been demonstrated experimentally and theoretically in both one- (1D) and two-dimensional (2D) periodic lattices. Such phenomena include (but are not limited to) dipole solitons, vortex solitons, and soliton trains [6–8]. These solitons are usually considered theoretically as bifurcations from the Bloch-band edges into the band gaps [9,10]. Similarly, solitons can sometimes be found in near-periodic and complex media [11,12]. While most work has tended to focus on seeking different types of solitons and studying their properties, nevertheless, the overall dynamics of wave envelopes, beyond localized modes, is also very important. Unfortunately, the complete analytical understanding of the dynamics is still open.

The standard mathematical model that governs electromagnetic wave propagating in periodic nonlinear media or condensates trapped in periodic optical lattices is the nonlinear Schrödinger (NLS) equation with a periodic potential. In this description, the local minima of the periodic potential, which are called sites, play an important role in the structure of the Bloch modes and the associated dispersion relations. These sites are the positions of the potential wells; and, in optics, they have increased refractive index, hence, the electric field is attracted to them. In BEC, the condensates localize near these sites, since they are near the minima of the potential wells. Mathematically speaking, the Bloch modes show increased intensity around the sites. If the potential well at each site is very deep, the intensity of the Bloch modes becomes more and more localized around the sites. This is related to the so-called tight binding (TB) approximation. The interactions of Bloch modes are mainly determined by the behavior of the nearby sites. Thus, the site distribution becomes very important in classifying 2D lattices. Roughly speaking, there are simple 2D lattices and nonsimple 2D lattices. A simple lattice contains one site per unit cell, while a nonsimple lattice contains more than one site per unit cell. Square lattices and equilateral triangular lattices are typical simple lattices. A common and naturally existing nonsimple lattice is the honeycomb lattice, which has two sites in each unit cell. An important physical application of these lattices is the material graphene, which has a honeycomb lattice structure. Ablowitz and Zhu studied the dynamics in simple nonlinear periodic media and developed a unified description of the wave envelope dynamics [13]. In this paper, we develop the analysis associated with nonsimple honeycomb lattices.

Honeycomb lattices can lead to significantly different results than found in simple lattices. Unlike simple lattices, where different dispersion surfaces typically either separate completely or intersect, it is found that, due to the underlying symmetries in honeycomb lattices, the dispersion relation of the associated Bloch theory, may also have isolated degenerate points in the first band, where two dispersion surfaces touch each other. These points are called Dirac points (sometimes referred to as, diabolical points [14]); and, in the neighborhood of the Dirac points, the dispersion surfaces have a conical

*Yi.Zhu@colorado.edu

structure. The existence of the Dirac points plays a very important role in the novel properties of graphene [15]. Due to the conical structure of the dispersion relations, from lattice NLS equations, one can find nonlinear Dirac wave systems, which govern the wave dynamics [16,17]. There are interesting phenomena associated with these Dirac systems. An example in optics is the conical diffraction, where a narrow beam transforms into bright expanding rings [14,16,18]. Honeycomb lattices also admit various types of band-gap solitons, which are due to the effect of nonlinearity like other 2D periodic lattices (cf. Refs. [19,20]). In BEC, honeycomb background lattices may also lead to interesting phenomena [17].

If the honeycomb lattice is deformed, and the symmetries are broken, then the dispersion relation (first band) will change as well as the associated wave envelope dynamics [21]. Under some conditions, the first band with two branches, which originally touch, can split into two bands with a corresponding band gap formed between the two branches. Thus, the dynamics of the wave envelope can change dramatically.

In this paper, we employ a discrete approximation to describe the envelope dynamics in general 2D honeycomb lattices. This technique has been used in 1D problems [22,23]. We first derive the linear dispersion relation in the lowest band, which can have two touching branches. If the the honeycomb lattice is appropriately deformed, there exist two Dirac points in the Brillouin zone. With the understanding of the linear dispersion relation, the nonlinear dynamics are then governed by a unified discrete wave system. At the locations where the Bloch modes touch, we find a nonlinear discrete Dirac system. From the discrete Dirac system in the continuous limit, the dynamics of the wave envelope is governed by a scaled nonlinear Dirac system. Coupled nonlinear Dirac systems can also be obtained where the coupling is developed between conjugate Dirac points. In another limit from the general discrete system, the wave envelope away from the Dirac points is governed by an NLS equation. We also study the case when the input beam is composed of two Bloch-mode envelopes, which correspond to the upper and lower branches, respectively. In certain cases, the dynamics is found to be governed by a coupled NLS system.

II. HONEYCOMB LATTICES AND THEIR DISPERSION RELATIONS

Electromagnetic waves that propagate in an inhomogeneous Kerr nonlinear medium are often described by the 2D NLS equation, written in dimensionless form

$$i\psi_z + \nabla^2\psi - V(\mathbf{r})\psi + \sigma|\psi|^2\psi = 0, \tag{1}$$

where $\mathbf{r} = (x,y)$ is the transverse coordinate, z is the propagation direction, $V(\mathbf{r})$ represents the spatial varying of the refractive index, which is often periodic, and σ is the nonlinear coefficient, which is positive for focusing nonlinearity and is negative for defocusing nonlinearity. This model also arises in ultracold atoms, BEC, trapped in a periodic lattice where the NLS with an external potential is often called the Gross-Pitaevskii equation.

A 2D periodic function has two periods along two different directions, which we call primitive lattice vectors. We denote them as $\mathbf{v}_1$ and $\mathbf{v}_2$. These two vectors can generate a set of lattice vectors $\mathbb{P} = \{m\mathbf{v}_1 + n\mathbf{v}_2 : m,n \in \mathbb{Z}\}$, and, then, for any $\mathbf{v} \in \mathbb{P}$, $V(\mathbf{r}+\mathbf{v}) = V(\mathbf{r})$. In the dual spectrum space, we denote $\mathbf{k}_1$ and $\mathbf{k}_2$ as the two primitive reciprocal lattice vectors and we denote $\mathbb{G} = \{m\mathbf{k}_1 + n\mathbf{k}_2 : m,n \in \mathbb{Z}\}$ as the set of reciprocal lattice vectors. The relation between lattice and reciprocal lattices is $\mathbf{v}_m \cdot \mathbf{k}_n = 2\pi\delta_{mn}, m,n = 1,2$. The two primitive lattice vectors $\mathbf{v}_1$ and $\mathbf{v}_2$ form a parallelogram, which is termed the unit cell of the physical lattice, which we denote Ω. Due to its periodicity, the potential $V(\mathbf{r})$ is completely determined by the information in Ω. Similarly, the parallelogram determined by the two reciprocal primitive lattice vectors $\mathbf{k}_1$ and $\mathbf{k}_2$ is the unit cell of the reciprocal lattice, which we denote Ω'.

In this paper, we will only study honeycomb lattices. A honeycomb lattice can be generated by interfering three plane waves for which the following lattice potential is a prototype:

$$V(\mathbf{r}) = \frac{V_0}{(1+\eta_1+\eta_2)^2}[|e^{ik_0\mathbf{b}_1\cdot\mathbf{r}} + \eta_1 e^{ik_0\mathbf{b}_2\cdot\mathbf{r}} + \eta_2 e^{ik_0\mathbf{b}_3\cdot\mathbf{r}}|^2 - (1+\eta_1+\eta_2)^2], \tag{2}$$

where $\mathbf{b}_1 = (0,1)$, $\mathbf{b}_2 = (-\frac{\sqrt{3}}{2}, -\frac{1}{2})$, and $\mathbf{b}_3 = (\frac{\sqrt{3}}{2}, -\frac{1}{2})$; $V_0 > 0$ is the lattice intensity; η_1 and η_2 are relative intensities of the plane waves. For simplicity, we only consider the case where $\eta_1 = \eta_2 = \eta > 0$ in this paper. In order to form a honeycomb lattice, the condition $\eta > \frac{1}{2}$ should be satisfied.

As with other 2D periodic functions, honeycomb lattices have two primitive lattice vectors. However, unlike simple 2D lattices, a honeycomb lattice has two sites in one unit cell. So, we need two starting points to generate all sites by the periodicity. The site distributions are displayed in Fig. 1. It is seen that the lattice has two sites in one cell, which we call A and B sites. The dots represent A sites, and the circles represent B sites. All A sites form a triangular lattice, and all B sites form another triangular lattice. We denote $A_\mathbf{0}$ and $B_\mathbf{0}$ as the positions of the starting sites. So, $A_\mathbf{v} = A_\mathbf{0} + \mathbf{v}$ and $B_\mathbf{v} = B_\mathbf{0} + \mathbf{v}$ are the positions of A and B sites in cell $\mathbf{v}$. The shift vector between A and B sites in one cell is defined as $\mathbf{d}_0 = A_\mathbf{0} - B_\mathbf{0}$. We also denote two other vectors $\mathbf{d}_1 = \mathbf{d}_0 + \mathbf{v}_1$ and $\mathbf{d}_2 = \mathbf{d}_0 + \mathbf{v}_2$. Then, all A sites have three nearest B sites, and the shift vectors are $\mathbf{d}_0$, $\mathbf{d}_1$, and $\mathbf{d}_2$. If $\eta = 1$, they all have the same length, and this is a standard (undeformed) honeycomb lattice. However, for a deformed honeycomb lattice, $\eta \neq 1$ and $|\mathbf{d}_1| = |\mathbf{d}_2| \neq |\mathbf{d}_0|$.

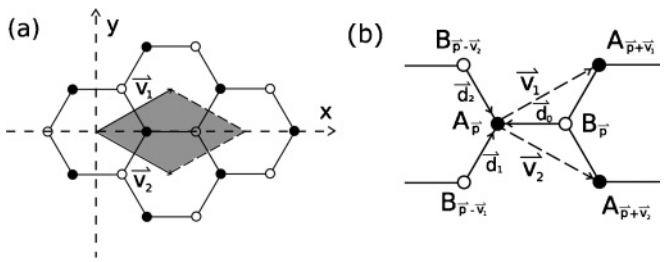

FIG. 1. (a) A honeycomb lattice. (b) Characteristic vectors and sites around a site. The shadow region in (a) is the primitive unit cell Ω.

The characteristic vectors of the honeycomb lattice Eq. (2) are then,

$$\mathbf{v}_1 = l\left(\frac{\sqrt{3}}{2},\frac{1}{2}\right), \quad \mathbf{v}_2 = l\left(\frac{\sqrt{3}}{2},-\frac{1}{2}\right),$$
$$\mathbf{k}_1 = \frac{4\pi}{\sqrt{3}l}\left(\frac{1}{2},\frac{\sqrt{3}}{2}\right), \quad \mathbf{k}_2 = \frac{4\pi}{\sqrt{3}l}\left(\frac{1}{2},-\frac{\sqrt{3}}{2}\right),$$
$$A_{\mathbf{0}} = \frac{\sqrt{3}}{2\pi}l\left(\pi - \arccos\left(\frac{1}{2\eta}\right),0\right),$$
$$B_{\mathbf{0}} = \frac{\sqrt{3}}{2\pi}l\left(\pi + \arccos\left(\frac{1}{2\eta}\right) - 2\pi,0\right),$$

where $l = \frac{4\pi}{3k_0}$ is the lattice constant (i.e., the length of the primitive lattice vectors). These values are found from the geometric location of the minima of the lattice and periodicity. The shift vectors from its three nearest B sites to the A site are

$$\mathbf{d}_0 = \frac{\sqrt{3}}{2\pi}l\left(-2\arccos\left(\frac{1}{2\eta}\right),0\right),$$
$$\mathbf{d}_1 = \frac{\sqrt{3}}{2\pi}l\left(\pi - 2\arccos\left(\frac{1}{2\eta}\right),\frac{\sqrt{3}}{3}\pi\right),$$
$$\mathbf{d}_2 = \frac{\sqrt{3}}{2\pi}l\left(\pi - 2\arccos\left(\frac{1}{2\eta}\right),-\frac{\sqrt{3}}{3}\pi\right).$$

It is seen that $|\mathbf{d}_0| = |\mathbf{d}_1| = |\mathbf{d}_2| = \frac{\sqrt{3}}{3}l$, when $\eta = 1$.

It is also noted that the asymptotic expansion of the potential near the sites is

$$V(\mathbf{r}) \approx V_0\left\{\frac{9k_0^2}{4(1+2\eta)^2}\left[\frac{(4\eta^2-1)}{3}(x-x_0)^2 + (y-y_0)^2\right] - 1\right\}, \tag{3}$$

where (x_0, y_0) is the coordinate of some site. Note that, if $\eta = 1$, the potential is locally harmonic. Otherwise, there is an anisotropy ratio $\frac{(4\eta^2-1)}{3}$.

If the wave intensity $|\psi(z,\mathbf{r})|$ is infinitesimal, or equivalently, σ is infinitesimal, the nonlinear term can be omitted, and we get a linear Schrödinger equation with a periodic potential. It can be solved by seeking the propagating solution $\psi(z,\mathbf{r}) = \varphi(\mathbf{r})e^{-i\mu z}$, where μ is called the propagation constant. Then, we obtain a linear eigenvalue problem:

$$\mu\varphi + \nabla^2\varphi - V(\mathbf{r})\varphi = 0. \tag{4}$$

According to the Bloch theorem, the eigenfunction of the the eigenvalue problem Eq. (4), called the Bloch mode or the Bloch wave, has the $\mathbf{k}$-dependent form

$$\varphi(\mathbf{r};\mathbf{k}) = e^{i\mathbf{k}\cdot\mathbf{r}}U(\mathbf{r};\mathbf{k}), \tag{5}$$

where $U(\mathbf{r};\mathbf{k})$ has the same periodicity as the potential $V(\mathbf{r})$ for any $\mathbf{k}$ [i.e., $U(\mathbf{r}+\mathbf{v};\mathbf{k}) = U(\mathbf{r};\mathbf{k})$ for any $\mathbf{v} \in \mathbb{P}$]. The eigenvalue $\mu = \mu(\mathbf{k})$ is the dispersion relation. In this paper, we use the convention that $\mu(\mathbf{k})$ is a periodic function of $\mathbf{k}$ and so is the associated Bloch mode $\varphi(\mathbf{r};\mathbf{k})$ [24]. The two periods are $\mathbf{k}_1$ and $\mathbf{k}_2$. So, the dispersion relation $\mu(\mathbf{k})$ is defined in the Brillouin zone Ω' and usually can have multiple band structures. There may exist band gaps between two dispersion surfaces, where bounded Bloch modes are not allowed.

Due to the periodicity of $\varphi(\mathbf{r};\mathbf{k})$ over $\mathbf{k}$, one can represent $\varphi(\mathbf{r};\mathbf{k})$ as a Fourier series,

$$\varphi(\mathbf{r};\mathbf{k}) = \sum_{\mathbf{v}} \phi(\mathbf{r}-\mathbf{v})e^{i\mathbf{k}\cdot\mathbf{v}}, \tag{6}$$

where $\phi(\mathbf{r}-\mathbf{v})$ defined as

$$\phi(\mathbf{r}-\mathbf{v}) = \frac{1}{|\Omega'|}\int_{\Omega'} \varphi(\mathbf{r};\mathbf{k})e^{-i\mathbf{k}\cdot\mathbf{v}}\,d\mathbf{k} \tag{7}$$

is the so-called Wannier function [25]; here and afterward, the sum over $\mathbf{v}$ means $\mathbf{v}$ takes all values in $\mathbb{P}$ (i.e., $\mathbf{v} = m\mathbf{v}_1 + n\mathbf{v}_2$) for all $m,n \in \mathbb{Z}$. Bloch modes can be constructed by Wannier functions through Eq. (6), and Wannier functions can be constructed by Bloch modes through Eq. (7). Wannier functions are independent of $\mathbf{k}$. From the TB approximation, the corresponding Bloch modes are mainly determined by the local behavior of the potential near the sites. This leads to Wannier functions being exponentially localized. As opposed to simple lattices where the Wannier function is a single localized function, the Wannier functions Eq. (7) for honeycomb lattices are instead composed of two localized functions.

In order to approximately compute the corresponding Wannier function, we write the potential in the form

$$V(\mathbf{r}) = \sum_{\mathbf{v}}[V_1(\mathbf{r}-\mathbf{v}) + V_2(\mathbf{r}-\mathbf{v})], \tag{8}$$

where $V_1(\mathbf{r})$ and $V_2(\mathbf{r})$ represent the potentials at sites $A_{\mathbf{0}}$ and $B_{\mathbf{0}}$; $V_2(\mathbf{r}) = V_1(\mathbf{r}+\mathbf{d}_0)$, where we recall that $\mathbf{d}_0 = A_{\mathbf{0}} - B_{\mathbf{0}}$. It is convenient to introduce the notation:

$$\Delta V_s(\mathbf{r}) = V(\mathbf{r}) - V_s(\mathbf{r}) = \sum_{\mathbf{v}\neq\mathbf{0}}[V_s(\mathbf{r}-\mathbf{v}) + V_j(\mathbf{r}-\mathbf{v})] + V_j(\mathbf{r}), \quad j \neq s.$$

Usually, $V_s(\mathbf{r}), s = 1,2$ can be approximated by rapidly decaying functions. This approximation does not change the Bloch modes and the associated dispersion relation in the TB limit (via WKB theory) and leads to detailed analytical results. This technique has been successfully used in simple lattices [13]. In order to give the asymptotic expansion Eq. (3), a simple approximation is

$$V_s(\mathbf{r}) \approx -V_0 e^{\hat{k}^2[c^2(x-x_0)^2+(y-y_0)^2]}, \quad s = 1,2,$$

where $c^2 = \frac{(4\eta^2-1)}{3}$ and $\hat{k}^2 = \frac{9k_0^2}{4(1+2\eta)^2}$. It is noted that the subsequent analysis is independent of this approximation. However, this approximation can give analytical results. All detailed calculations are in the Appendix.

For each rapidly decaying $V_s(\mathbf{r})$, we can define the corresponding orbital,

$$\mathcal{H}_s^{\mathbf{0}}\phi_s \equiv [\nabla^2 - V_s(\mathbf{r})]\phi_s(\mathbf{r}) = -E\phi_s(\mathbf{r}),$$

where, for any $\mathbf{v} \in \mathbb{P}$,

$$\mathcal{H}_s^{\mathbf{v}} = \nabla^2 - V_s(\mathbf{r}-\mathbf{v}),$$

and E is called the orbital energy. It is noted that $\phi_2(\mathbf{r}) = \phi_1(\mathbf{r}+\mathbf{d}_0)$, since $V_2(\mathbf{r}) = V_1(\mathbf{r}+\mathbf{d}_0)$.

In this paper, we only consider the lowest band in detail, so we only need to consider the ground state of $\mathcal{H}_s^{\mathbf{v}}$. However, the basic analysis presented in the following is valid for the

higher bands as well. In the higher bands, the corresponding eigenspace of $\mathcal{H}_s^{\mathbf{v}}$ is usually degenerate, so one should consider the degeneracy in some detail. Interested readers can combine the following analysis with the analysis already performed in simple lattices to study higher band dynamics [13].

The honeycomb potential has two wells in a unit cell, and then, the Wannier function in Eq. (7) is a linear combination of the two associated orbitals, that is,

$$\phi(\mathbf{r}) = \alpha\phi_1(\mathbf{r}) + \beta\phi_2(\mathbf{r}), \tag{9}$$

then, the Bloch mode has the form

$$\varphi(\mathbf{r};\mathbf{k}) \approx \sum_{\mathbf{v}} [\alpha\phi_1(\mathbf{r}-\mathbf{v}) + \beta\phi_2(\mathbf{r}-\mathbf{v})]e^{i\mathbf{k}\cdot\mathbf{v}}, \tag{10}$$

where α and β are two parameters, which are determined by the detailed calculations given later. It is noted that both ϕ_1 and ϕ_2 are real and normalized to unity (i.e., $\int \phi_1\phi_1\, d\mathbf{r} = \int \phi_2\phi_2\, d\mathbf{r} = 1$), and the sums over $\mathbf{v}$ are understood to be over A sites when working with the ϕ_1 function and over B sites when dealing with ϕ_2.

We first rewrite the eigenvalue problem Eq. (4) in the form

$$\left(\mathcal{H}_s^{\mathbf{0}} + E\right)\varphi(\mathbf{r}) = [E - \mu + \Delta V_s(\mathbf{r})]\varphi(\mathbf{r}) \equiv F_s. \tag{11}$$

Note that the operator $\mathcal{H}_s^{\mathbf{0}} + E$ has a 1D null-space, which is spanned by $\phi_s(\mathbf{r})$ for $s = 1,2$. Then, the Fredholm alternative requires that the right-hand side be orthogonal to $\phi_s(\mathbf{r})$, that is,

$$\int F_s\phi_s(\mathbf{r})\, d\mathbf{r} = \int [E - \mu + \Delta V_s(\mathbf{r})]\varphi(\mathbf{r})\phi_s(\mathbf{r})\, d\mathbf{r} = 0,$$
$$s = 1,2.$$

By substituting the earlier Bloch mode Eq. (10) into the preceding Fredholm conditions yields that

$$(\mu - E)\left[\sum_{\mathbf{v}} \kappa_{11}(\mathbf{v})e^{i\mathbf{k}\cdot\mathbf{v}}\right]\alpha - \left[\sum_{\mathbf{v}} \lambda_{11}(\mathbf{v})e^{i\mathbf{k}\cdot\mathbf{v}}\right]\alpha$$
$$+ (\mu - E)\left[\sum_{\mathbf{v}} \kappa_{12}(\mathbf{v})e^{i\mathbf{k}\cdot\mathbf{v}}\right]\beta - \left[\sum_{\mathbf{v}} \lambda_{12}(\mathbf{v})e^{i\mathbf{k}\cdot\mathbf{v}}\right]\beta = 0,$$

and

$$(\mu - E)\left[\sum_{\mathbf{v}} \kappa_{22}(\mathbf{v})e^{i\mathbf{k}\cdot\mathbf{v}}\right]\beta - \left[\sum_{\mathbf{v}} \lambda_{22}(\mathbf{v})e^{i\mathbf{k}\cdot\mathbf{v}}\right]\beta$$
$$+ (\mu - E)\left[\sum_{\mathbf{v}} \kappa_{21}(\mathbf{v})e^{i\mathbf{k}\cdot\mathbf{v}}\right]\alpha - \left[\sum_{\mathbf{v}} \lambda_{21}(\mathbf{v})e^{i\mathbf{k}\cdot\mathbf{v}}\right]\alpha = 0,$$

where

$$\kappa_{ij}(\mathbf{v}) = \int \phi_i(\mathbf{r})\phi_j(\mathbf{r}-\mathbf{v})\, d\mathbf{r},$$
$$\lambda_{ij}(\mathbf{v}) = \int \phi_i(\mathbf{r})\, \Delta V_j\, \phi_j(\mathbf{r}-\mathbf{v})\, d\mathbf{r}.$$

Now, the original eigenvalue problem Eq. (4) is converted into a linear system for α,β. The system has nontrivial solutions if and only if the determinant of the coefficient matrix is zero. This determines the dispersion relation, and the solutions of the linear system (i.e., the relation of α and β) give the eigenmodes Eqs. (4)–(10).

The preceding linear system can be greatly simplified in the TB limit. Note that $\kappa_{ij}(\mathbf{v})$ and $\lambda_{ij}(\mathbf{v})$ exponentially decay as $|\mathbf{v}| \to +\infty$. We only consider on-site and nearest-neighbor interactions, while other interactions are very small. More specifically, for site $A_{\mathbf{0}}$, we only keep its interactions with itself and its three nearest neighbors, which are B sites at $B_{\mathbf{0}}$, $B_{-\mathbf{v}_1}$, and $B_{-\mathbf{v}_2}$; for the site $B_{\mathbf{0}}$, its three nearest neighbors are A sites at $A_{\mathbf{0}}$, $A_{\mathbf{v}_1}$, and $A_{\mathbf{v}_2}$.

From the symmetries of the potential, we find that

$$c_0 = \lambda_{11}(\mathbf{0}) = \lambda_{22}(\mathbf{0}),$$
$$c_1 = \kappa_{12}(\mathbf{0}) = \kappa_{21}(\mathbf{0}) = \frac{1}{\rho_1}\kappa_{12}(-\mathbf{v}_s) = \frac{1}{\rho_1}\kappa_{21}(\mathbf{v}_s),$$
$$c_2 = \lambda_{12}(\mathbf{0}) = \lambda_{21}(\mathbf{0}) = \frac{1}{\rho_2}\lambda_{12}(-\mathbf{v}_s) = \frac{1}{\rho_2}\lambda_{21}(\mathbf{v}_s),$$

where $\rho_s > 0, s = 1,2$ denote the ratio of the asymmetry of three nearest-neighbor interactions under deformations and $\rho_s = 1$ when the lattice is not deformed (i.e., $\eta = 1$).

Thus, the previous system becomes

$$\begin{bmatrix} \mu - E - c_0 & (\mu - E)c_1\gamma_1(\mathbf{k}) - c_2\gamma_2(\mathbf{k}) \\ (\mu - E)c_1\gamma_1^*(\mathbf{k}) - c_2\gamma_2^*(\mathbf{k}) & \mu - E - c_0 \end{bmatrix}$$
$$\times \begin{pmatrix} \alpha \\ \beta \end{pmatrix} = \begin{pmatrix} 0 \\ 0 \end{pmatrix}, \tag{12}$$

where

$$\gamma_s(\mathbf{k}) = 1 + \rho_s e^{-i\mathbf{k}\cdot\mathbf{v}_1} + \rho_s e^{-i\mathbf{k}\cdot\mathbf{v}_2}, \quad s = 1,2. \tag{13}$$

The preceding system Eq. (12) has nonzero solutions if and only if the determinant is zero, which gives the dispersion relation:

$$(\mu - E - c_0)^2 = |(\mu - E)c_1\gamma_1(\mathbf{k}) - c_2\gamma_2(\mathbf{k})|^2.$$

Note that $c_1 \ll 1$, so the dispersion relation is

$$(\mu - E - c_0)^2 \approx |c_0c_1\gamma_1(\mathbf{r}) - c_2\gamma_2(\mathbf{r})|^2. \tag{14}$$

The preceding equation Eq. (14) defines two dispersion relation branches written in a unified form ($j = 1,2$),

$$\mu_j(\mathbf{k}) \approx E + c_0 + (-1)^j C|\gamma(\mathbf{k})|, \tag{15}$$

where we denote

$$C = c_0c_1 - c_2 > 0,$$
$$\gamma(\mathbf{k}) = 1 + \rho e^{-i\mathbf{k}\cdot\mathbf{v}_1} + \rho e^{-i\mathbf{k}\cdot\mathbf{v}_2},$$

and

$$\rho = \frac{c_0c_1\rho_1 - c_2\rho_2}{c_0c_1 - c_2} > 0.$$

All parameters in the previous equations can be calculated analytically in the TB approximation. Details can be found in the Appendix. For the undeformed honeycomb lattice (i.e., $\eta = 1$, $\rho = 1$).

The eigenmode that corresponds to $\mu_j(\mathbf{k})$ then satisfies

$$\begin{bmatrix} (-1)^j|\gamma(\mathbf{k})| & \gamma(\mathbf{k}) \\ \gamma^*(\mathbf{k}) & (-1)^j|\gamma(\mathbf{k})| \end{bmatrix}\begin{pmatrix} \alpha \\ \beta \end{pmatrix} = \begin{pmatrix} 0 \\ 0 \end{pmatrix}. \tag{16}$$

So far, we have found the dispersion relation for the lowest band and the associated Bloch modes. The linear dynamics associated with the lowest band is completely solved due to the completeness of the Bloch modes [26].

Whereas the first band of the dispersion relation for simple lattices is usually simple when $V_0 \ll 1$ [13], this is not usually the case for honeycomb lattices. As indicated by Eq. (15), we find the first band for honeycomb lattices has two branches. This is called Davydov splitting in the theory of molecular excitons [27]. This is due to having multiple sites per unit cell.

Since $\mu_1(\mathbf{k}) \leqslant \mu_2(\mathbf{k})$, we call $\mu_1(\mathbf{k})$ the lower branch and $\mu_2(\mathbf{k})$ the upper branch. If $\gamma(\mathbf{k})$ is real and positive, for instance, $\mathbf{k} = \mathbf{0}$, we get $\alpha = \beta$ for the lower branch and $\alpha = -\beta$ for the upper branch; so the lower branch corresponds to a symmetric Bloch mode, and the upper branch corresponds to an antisymmetric Bloch mode. However, $\gamma(\mathbf{k})$ is usually nonreal, in which case, α and β have a more complex relationship.

If $\rho < \frac{1}{2}$, $|\gamma(\mathbf{k})| > 0$ and $\mu_1(\mathbf{k}) < \mu_2(\mathbf{k})$ for any $\mathbf{k} \in \mathbb{R}^2$, thus, there exists a gap between the upper and lower branches. So, they are considered to belong to two different bands. Note that ρ measures the asymmetry of three nearest-neighbor interactions and depends on both V_0 and the asymmetric parameter η. For a fixed V_0, the smaller η is, that is, the greater the deformation, the smaller the ρ . In this paper, we only consider the case where $\rho > \frac{1}{2}$, then $\gamma(\mathbf{k})$ always has two isolated zeros in the Brillouin zone Ω'. We call these two zeros $\mathbf{K}$ and $\mathbf{K}'$, which are referred to as Dirac points. Here, $\mathbf{K} = \frac{2}{l}(0, \pi - \arccos\frac{1}{2\rho})$ and $\mathbf{K}' = -\mathbf{K}$. The two branches touch each other at these two Dirac points, and they belong to the same band. The existence of the Dirac points are due to the underlying symmetries of the honeycomb lattices. Interesting phenomena are associated with the Dirac points.

The Brillouin zone and the dispersion relation is displayed in Fig. 2. In (a), the Brillouin zone is the shadowed parallelogram. However, in the literature, the hexagon surrounded by dotted lines is often used as the Brillouin zone. The parallelogram and the hexagon are actually equivalent due to the periodicity. In (b), we plot the dispersion relation in an extended Brillouin zone (which corresponds to the rectangle surrounded by dashed lines) for convenience. It is seen that there exist Dirac points. In that figure, it seems that there

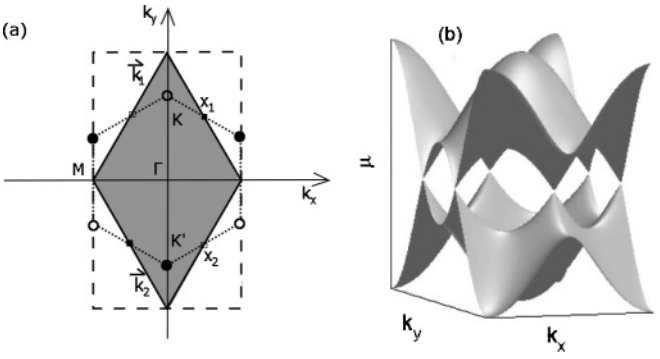

FIG. 2. (a) Brillouin zone of the honeycomb lattice and special points. (b) The dispersion relation of the lowest band. The shadow region in (a) is the Brillouin zone. It is equivalent to the hexagon surrounded by dotted lines, which is often used as the Brillouin zone instead in the literature.

are six touching points, but actually, there are only two independent Dirac points. For example, in (a), all dots are equivalent to the $\mathbf{K}'$ point, and all circles are the $\mathbf{K}$ point due to the periodicity of $\mu(\mathbf{k})$.

If $\mathbf{k}$ is not a Dirac point, the two branches have different values, and each one has a 1D eigenspace, and the corresponding eigenfunction is determined by solving the linear system Eq. (16). If $\mathbf{k} = \mathbf{K}, \mathbf{K}'$, $\mu_1 = \mu_2 = E + c_0$. The upper and lower branches merge to the same value. Thus, the eigenvalue has multiplicity 2. Then, to solve the eigenproblem, Eq. (16) implies that both α, β in the Bloch mode Eq. (10) are free. So, the eigenspace that corresponds to $\mu = E + c_0$ is 2D. A convenient set of two linearly independent Bloch modes is given by

$$\varphi^{(1)}(\mathbf{r}; \mathbf{k}) \approx \sum_{\mathbf{v}} \phi_1(\mathbf{r} - \mathbf{v}) e^{i\mathbf{k}\cdot\mathbf{v}}, \tag{17}$$

$$\varphi^{(2)}(\mathbf{r}; \mathbf{k}) \approx \sum_{\mathbf{v}} \phi_2(\mathbf{r} - \mathbf{v}) e^{i\mathbf{k}\cdot\mathbf{v}}, \tag{18}$$

where $\mathbf{k}$ only takes the values $\mathbf{K}$ or $\mathbf{K}'$. Then, $\varphi^{(1)}$ represents the Bloch mode that corresponds to the A component, while $\varphi^{(2)}$ represents the Bloch mode that corresponds to the B component. These two Bloch modes are displayed in Fig. 3, where it is seen that Bloch mode $\varphi^{(1)}(\mathbf{r}; \mathbf{K})$ has intensity only near the A sites, while the Bloch mode $\varphi^{(2)}(\mathbf{r}; \mathbf{K})$ has intensity only near B sites. In general, an arbitrary Bloch mode is a linear combination of these two Bloch modes.

III. DYNAMICS OF DISCRETE BLOCH-MODE ENVELOPES—A UNIFIED NONLINEAR DISCRETE ENVELOPE EQUATION

Understanding of the linear dispersion relation allows us to describe the wave envelope dynamics in the presence of weak (not infinitesimal) nonlinearity. A discrete Bloch-mode envelope has the form

$$\psi \sim \sum_{\mathbf{v}} [a_{\mathbf{v}} \phi_1(\mathbf{r} - \mathbf{v}) + b_{\mathbf{v}} \phi_2(\mathbf{r} - \mathbf{v})] e^{i\mathbf{k}\cdot\mathbf{v}}. \tag{19}$$

Here, $a_{\mathbf{v}}$ and $b_{\mathbf{v}}$ are scaled Bloch envelopes that correspond to the different A and B sites; thus, $a_{\mathbf{v}}$ is defined on the A site and similarly for $b_{\mathbf{v}}$. Under evolution, the envelopes $a_{\mathbf{v}}(Z)$ and $b_{\mathbf{v}}(Z)$ vary slowly in z, here, $Z = \varepsilon z$ (the small parameter ε will be determined later).

To leading order, the evolution of the envelope is taken to be of the form

$$\psi \sim \left\{ \sum_{\mathbf{v}} [a_{\mathbf{v}}(Z) \phi_1(\mathbf{r} - \mathbf{v}) + b_{\mathbf{v}}(Z) \phi_2(\mathbf{r} - \mathbf{v})] e^{i\mathbf{k}\cdot\mathbf{v}} \right\} e^{-i(E + c_0)z}. \tag{20}$$

It is noted that the input Bloch-mode envelope in Eq. (19) is usually composed of two components: One is related to the lower branch with propagating phase $e^{-i\mu_1 z}$, and the other is related to the upper branch with propagating phase $e^{-i\mu_2 z}$. Since the difference is order $O(C)$, which is very small, they all have the propagation constant $E + c_0$ to leading order. The corrections of the propagation constants are included in the envelopes.

By substituting the previous envelope approximation Eq. (20) into the lattice NLS equation, Eq. (1)

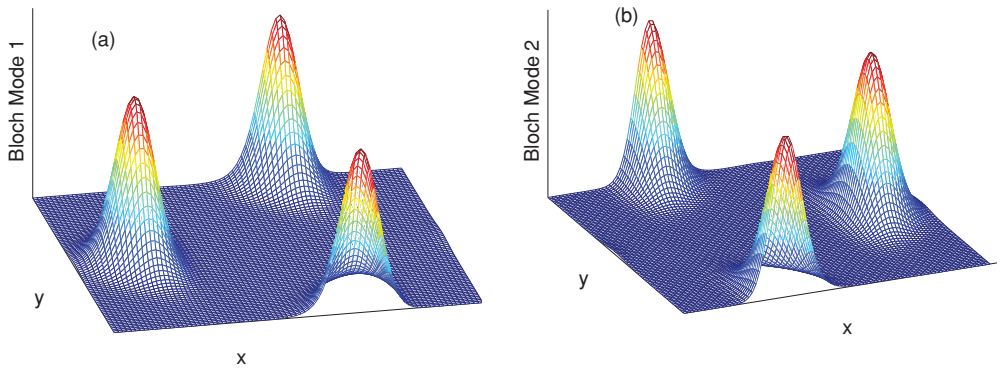

FIG. 3. (Color online) Two Bloch modes in the extended unit cell. (a) Bloch mode $\varphi^{(1)}(\mathbf{r};\mathbf{K})$. (b) Bloch mode $\varphi^{(2)}(\mathbf{r};\mathbf{K})$. The extended unit cell is the smallest rectangle that contains the primitive unit cell Ω.

implies

$$\begin{aligned}\left(\mathcal{H}_s^{\mathbf{p}}+E\right)\sum_{\mathbf{v}}&[a_{\mathbf{v}}(Z)\phi_1(\mathbf{r}-\mathbf{v})+b_{\mathbf{v}}(Z)\phi_2(\mathbf{r}-\mathbf{v})]e^{i\mathbf{k}\cdot\mathbf{v}}\\ =&-\sum_{\mathbf{v}}\left\{\varepsilon i\frac{da_{\mathbf{v}}}{dZ}+a_{\mathbf{v}}\left[c_0-\Delta V_s(\mathbf{r}-\mathbf{p})\right]\right\}\phi_1(\mathbf{r}-\mathbf{v})e^{i\mathbf{k}\cdot\mathbf{v}}\\ &-\sum_{\mathbf{v}}\left\{\varepsilon i\frac{db_{\mathbf{v}}}{dZ}+b_{\mathbf{v}}\left[c_0-\Delta V_s(\mathbf{r}-\mathbf{p})\right]\right\}\phi_2(\mathbf{r}-\mathbf{v})e^{i\mathbf{k}\cdot\mathbf{v}}\\ &-\sigma\left\{\sum_{\mathbf{v}}\left[a_{\mathbf{v}}\phi_1(\mathbf{r}-\mathbf{v})+b_{\mathbf{v}}\phi_2(\mathbf{r}-\mathbf{v})\right]e^{i\mathbf{k}\cdot\mathbf{v}}\right\}^2\\ &\times\left\{\sum_{\mathbf{v}}\left[a_{\mathbf{v}}\phi_1(\mathbf{r}-\mathbf{v})+b_{\mathbf{v}}\phi_2(\mathbf{r}-\mathbf{v})\right]e^{i\mathbf{k}\cdot\mathbf{v}}\right\}^*,\end{aligned}\tag{21}$$

where $\mathbf{p}\in\mathbb{P}$ is a lattice vector.

By applying the Fredholm conditions for the operators $\mathcal{H}_s^{\mathbf{p}}+E, s=1,2$, which have a 1D null-space, yields

$$\begin{aligned}\varepsilon i\frac{da_{\mathbf{p}}}{dZ}+(c_0c_1\mathcal{L}_1^--c_2\mathcal{L}_2^-)b_{\mathbf{p}}+\sigma g|a_{\mathbf{p}}|^2a_{\mathbf{p}}=0,\\ \varepsilon i\frac{db_{\mathbf{p}}}{dZ}+(c_0c_1\mathcal{L}_1^+-c_2\mathcal{L}_2^+)a_{\mathbf{p}}+\sigma g|b_{\mathbf{p}}|^2b_{\mathbf{p}}=0,\end{aligned}$$

where

$$\begin{aligned}\mathcal{L}_s^-b_{\mathbf{p}}=b_{\mathbf{p}}+\rho_sb_{\mathbf{p}-\mathbf{v}_1}e^{-i\mathbf{k}\cdot\mathbf{v}_1}+\rho_sb_{\mathbf{p}-\mathbf{v}_2}e^{-i\mathbf{k}\cdot\mathbf{v}_2},\\ \mathcal{L}_s^+a_{\mathbf{p}}=a_{\mathbf{p}}+\rho_sa_{\mathbf{p}+\mathbf{v}_1}e^{i\mathbf{k}\cdot\mathbf{v}_1}+\rho_sa_{\mathbf{p}+\mathbf{v}_2}e^{i\mathbf{k}\cdot\mathbf{v}_2},\end{aligned}$$

$s=1,2$, and $g=\int\phi_1^4\,d\mathbf{r}=\int\phi_2^4\,d\mathbf{r}$.

The preceding system can be rewritten in a nicer form (by taking the maximal balance $\varepsilon=C$),

$$i\frac{da_{\mathbf{p}}}{dZ}+\mathcal{L}^-b_{\mathbf{p}}+\frac{\sigma}{C}g|a_{\mathbf{p}}|^2a_{\mathbf{p}}=0,\tag{22}$$

$$i\frac{db_{\mathbf{p}}}{dZ}+\mathcal{L}^+a_{\mathbf{p}}+\frac{\sigma}{C}g|b_{\mathbf{p}}|^2b_{\mathbf{p}}=0,\tag{23}$$

where

$$\mathcal{L}^-b_{\mathbf{p}}=b_{\mathbf{p}}+\rho b_{\mathbf{p}-\mathbf{v}_1}e^{-i\mathbf{k}\cdot\mathbf{v}_1}+\rho b_{\mathbf{p}-\mathbf{v}_2}e^{-i\mathbf{k}\cdot\mathbf{v}_2},\tag{24}$$

$$\mathcal{L}^+a_{\mathbf{p}}=a_{\mathbf{p}}+\rho a_{\mathbf{p}+\mathbf{v}_1}e^{i\mathbf{k}\cdot\mathbf{v}_1}+\rho a_{\mathbf{p}+\mathbf{v}_2}e^{i\mathbf{k}\cdot\mathbf{v}_2}.\tag{25}$$

The previous system is a discrete evolution system, which governs the evolution of the Bloch wave envelope at a general location $\mathbf{k}$. It gives a unified description of the discrete envelope dynamics for the lowest band of a honeycomb lattice. One can carry out higher band dynamics via a similar procedure. This discrete system can describe the spatial scale at the order l (lattice constant). The slow time ε arises from the smallness of C, which also corresponds to the thickness of the dispersion band. It is valid in the TB limit. The nonlinearity can be chosen as the same order of C or smaller. Note that when we specialize to the Dirac point (i.e., either $\mathbf{k}=\mathbf{K},\mathbf{K}'$), then the foregoing discrete equations are regarded as a nonlinear discrete Dirac system.

It should be noted that the earlier discrete approach can be extended beyond the TB limit. If the potential intensity V_0 is not sufficiently large, the nearest-neighbor interaction approximation may not be adequate. In such cases, additional sites should be included in order to get more accurate approximations. This is outside the scope of this paper.

IV. CONTINUOUS LIMIT OF THE DISCRETE SYSTEM

For different values of $\mathbf{k}$, we find that the evolution of the envelopes can be very different. In this context, we consider a further limit, where $a_{\mathbf{v}}$ and $b_{\mathbf{v}}$ vary slowly with respect to how $\mathbf{v}$ changes. Namely, we consider the continuous limit of the preceding discrete systems for general values of $\mathbf{k}$. The envelopes can be written in the form $a(\mathbf{R})$ and $b(\mathbf{R})$, where $\mathbf{R}=(X,Y)=\nu\mathbf{r}$ represents the spatial coordinate of the slowly varying envelopes.

Before proceeding, we introduce the following notations: $\partial_m=\frac{\partial}{\partial\mathbf{r}_m}$ and $\nabla=(\partial_1,\partial_2)$; $\tilde{\partial}_m=\frac{\partial}{\partial\mathbf{R}_m}$ and $\tilde{\nabla}=(\tilde{\partial}_1,\tilde{\partial}_2)$; $\bar{\partial}_m=\frac{\partial}{\partial k_m}$ and $\bar{\nabla}=(\bar{\partial}_1,\bar{\partial}_2)$; $\bar{\partial}_{m,n}=\bar{\partial}_n\bar{\partial}_m$ and $\tilde{\partial}_{m,n}=\tilde{\partial}_n\tilde{\partial}_m$.

By using the Taylor expansion,

$$a_{\mathbf{p}+\mathbf{v}}=a_{\mathbf{p}}+\nu\mathbf{v}\cdot\tilde{\nabla}a+\frac{\nu^2}{2}\mathbf{v}\tilde{\mathbf{H}}\mathbf{v}^Ta+\cdots,$$

where $\tilde{\mathbf{H}}=\left(\begin{smallmatrix}\tilde{\partial}_{11}&\tilde{\partial}_{12}\\ \tilde{\partial}_{21}&\tilde{\partial}_{22}\end{smallmatrix}\right)$ is the Hessian matrix operator with respect to $\mathbf{R}$, we get

$$\mathcal{L}^-b_{\mathbf{p}}=b_{\mathbf{p}}\gamma-i\nu\bar{\nabla}\gamma\cdot\tilde{\nabla}b-\frac{\nu^2}{2}\sum_{m,n=1}^{2}\bar{\partial}_{m,n}\gamma\,\tilde{\partial}_{m,n}b+\cdots,$$

$$\mathcal{L}^+a_{\mathbf{p}}=a_{\mathbf{p}}\gamma^*-i\nu\bar{\nabla}\gamma^*\cdot\tilde{\nabla}a-\frac{\nu^2}{2}\sum_{m,n=1}^{2}\bar{\partial}_{m,n}\gamma^*\,\tilde{\partial}_{m,n}a+\cdots.$$

Hence, we have

$$i\,\partial_Z a + \left(\gamma\, b - i\nu\bar{\nabla}\gamma\cdot\tilde{\nabla}b - \frac{\nu^2}{2}\sum_{m,n=1}^{2}\bar{\partial}_{m,n}\gamma\,\tilde{\partial}_{m,n}b\right) + \frac{\sigma}{C}g|a|^2 a = 0, \tag{26a}$$

$$i\,\partial_Z b + \left(\gamma^* a - i\nu\bar{\nabla}\gamma^*\cdot\tilde{\nabla}a - \frac{\nu^2}{2}\sum_{m,n=1}^{2}\bar{\partial}_{m,n}\gamma^*\,\tilde{\partial}_{m,n}a\right) + \frac{\sigma}{C}g|b|^2 b = 0. \tag{26b}$$

This is the continuous limit of the discrete system, valid for any $\mathbf{k}$. It contains many scales. We still need to understand the behavior based on maximal balance, which depends critically on the location of $\mathbf{k}$.

A. Continuous Nonlinear Dirac System

In this section, we consider the case where $\mathbf{k}$ is one Dirac point (i.e., $\mathbf{k} = \mathbf{K}, \mathbf{K}'$). In this case, $\gamma(\mathbf{k}) = 0$, so $\mu_1 = \mu_2$, and the corresponding eigenspace is 2D. Therefore, the envelopes $a(\mathbf{R})$ and $b(\mathbf{R})$ are independent, and they correspond to Bloch modes $\varphi^{(1)}$ and $\varphi^{(2)}$, respectively.

At $\mathbf{k} = \mathbf{K}$, we find that

$$\bar{\nabla}\gamma = i(-\mathbf{v}_1\rho e^{-i\mathbf{K}\cdot\mathbf{v}_1} - \mathbf{v}_2\rho e^{-i\mathbf{K}\cdot\mathbf{v}_2}) = i\frac{\sqrt{3}l}{2}(1,\zeta i), \tag{27}$$

$$\bar{\nabla}\gamma^* = i(\mathbf{v}_1\rho e^{i\mathbf{K}\cdot\mathbf{v}_1} + \mathbf{v}_2\rho e^{i\mathbf{K}\cdot\mathbf{v}_2}) = i\frac{\sqrt{3}l}{2}(-1,\zeta i), \tag{28}$$

where $\zeta = \frac{\sqrt{4\rho^2-1}}{\sqrt{3}}$. We note that $\zeta = 1$ when the lattice is not deformed ($\eta = 1$ and $\rho = 1$).

By introducing a new variable $Z_1 = \nu Z$ (note $Z = \varepsilon z$), then after taking the maximal balance $\varepsilon\nu = C\nu = |\sigma|$, we get

$$i\,\partial_{Z_1} a + \frac{\sqrt{3}\,l}{2}(\partial_X + \zeta i\,\partial_Y)b + s(\sigma)g|a|^2 a = 0, \tag{29a}$$

$$i\,\partial_{Z_1} b + \frac{\sqrt{3}\,l}{2}(-\partial_X + \zeta i\,\partial_Y)a + s(\sigma)g|b|^2 b = 0, \tag{29b}$$

where $s(\sigma)$ is the sign of σ. The preceding system is the so-called (continuous) nonlinear Dirac system. It governs the dynamics of the envelopes associated with the Dirac point $\mathbf{K}$.

Similarly, if $\mathbf{k} = \mathbf{K}'$, the corresponding system is

$$i\,\partial_{Z_1} a + \frac{\sqrt{3}\,l}{2}(\partial_X - \zeta i\,\partial_Y)b + s(\sigma)g|a|^2 a = 0; \tag{30a}$$

$$i\,\partial_{Z_1} b + \frac{\sqrt{3}\,l}{2}(-\partial_X - \zeta i\,\partial_Y)a + s(\sigma)g|b|^2 b = 0. \tag{30b}$$

The two Dirac systems for $\mathbf{K}$ and $\mathbf{K}'$ are the same by just changing Y to $-Y$.

The original field of the lattice NLS equation Eq. (1) has the following form:

$$\psi(z,\mathbf{r}) \sim [a(C\nu z,\nu r)\varphi^{(1)}(\mathbf{r};\mathbf{k}) + b(C\nu z,\nu r)\varphi^{(2)}(\mathbf{r};\mathbf{k})]e^{-i(E+c_0)z},$$

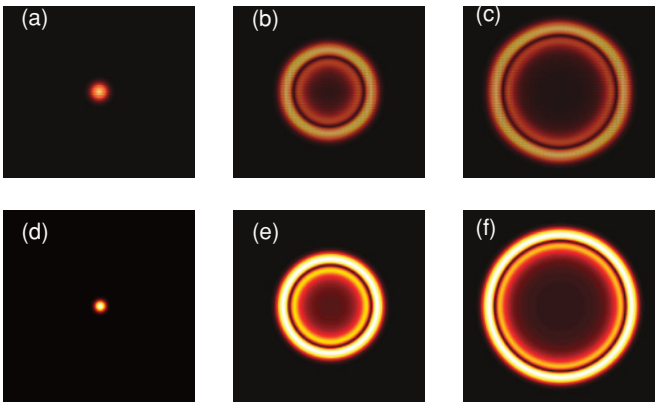

FIG. 4. (Color online) The propagation of a Gaussian Bloch-mode envelope associated with a Dirac point. Top: simulations of the lattice NLS equation Eq. (1); bottom: simulations of the nonlinear Dirac system Eq. (29). Here, only the a envelope is displayed.

where envelopes a and b satisfy the previous Dirac systems by depending on the k value.

An important associated phenomenon exhibited by the foregoing Dirac system is conical diffraction [16,18]. Here, we compare the numerical simulations of both the lattice NLS equation and the nonlinear Dirac system for certain parameters. The comparison is displayed in Fig. 4. The top panel is from the lattice NLS equation Eq. (1), where $V_0 = 100, k_0 = 32/\sqrt{3}, \eta = 1$, and $\sigma = 0.1$ with the initial condition as a certain Bloch mode multiplied by a wide Gaussian. The bottom panel is from the nonlinear Dirac system Eq. (29), where $s(\sigma) = 1$. Initially, a is a unit Gaussian, and b is zero. From the top panel, we see that a spot becomes two rings, which are separated by the so-called Poggendorff's dark ring [14]. The simulation of the nonlinear Dirac system gives a fine match.

The rings in the conical diffraction are actually elliptic if $\eta \neq 1$, where the ratio of axes is $\zeta = \frac{\sqrt{4\rho^2-1}}{\sqrt{3}}$. We also give two elliptic rings in Fig. 5. It is seen that the rings are not perfectly circular but elliptic. We also notice that the intensity along the rings is not uniform. The intensity is largest at the edges of the major axis and is smallest at the edges of the minor axis. It is noted that $\zeta \to 0$ as $\rho \to \frac{1}{2}$. So, if ζ has the same order as ν, a new maximal balance should be considered, and it leads to other interesting equations. This is outside the scope of this paper.

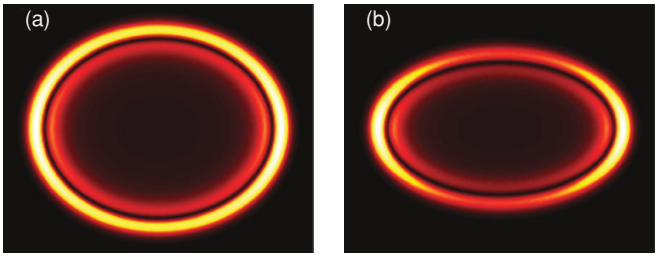

FIG. 5. (Color online) Circular rings become elliptic when honeycomb lattices are deformed. (a) $\rho = 0.8$, (b) $\rho = 0.6$.

B. NLS equations

In this section, the **k** value we are studying is well away from the Dirac points, then $\gamma(\mathbf{k}) \neq 0$; and, therefore, the dispersion relation is not degenerate. However, the input envelope Eq. (19) usually contains two components; one corresponds to the branch μ_1, and the other is associated with the branch μ_2. We first assume that the input envelope only contains one component. We will show that the governing equation is an effective NLS equation.

We expand the solution of the system Eq. (26) into a perturbation series:

$$a \sim a_0 + \nu a_1 + \nu^2 a_2 + \cdots,$$
$$b \sim b_0 + \nu b_1 + \nu^2 b_2 + \cdots.$$

We will use a multiscale expansion to derive the governing equations. We introduce a new scale $Z_1 = \nu Z$ (note $Z = \varepsilon z$) and will take the following balance:

$$\frac{|\sigma|}{C} = \nu^2.$$

Then, to leading order, we get the system:

$$i\,\partial_Z a_0 + \gamma b_0 = 0, \tag{31a}$$
$$i\,\partial_Z b_0 + \gamma^* a_0 = 0. \tag{31b}$$

It has the solution:

$$a_0 = P(Z_1,\mathbf{R})e^{i|\gamma|Z} + Q(Z_1,\mathbf{R})e^{-i|\gamma|Z}, \tag{32a}$$
$$b_0 = \frac{|\gamma|}{\gamma}P(Z_1,\mathbf{R})e^{i|\gamma|Z} - \frac{|\gamma|}{\gamma}Q(Z_1,\mathbf{R})e^{-i|\gamma|Z}. \tag{32b}$$

The leading-order solutions give the corrections to the propagation constants of the original field ψ in Eq. (20). Here, $P(Z_1,\mathbf{R})$ corresponds to the lower branch $\mu_1(\mathbf{k})$, and $Q(Z_1,\mathbf{R})$ corresponds to the upper branch $\mu_2(\mathbf{k})$.

We are interested in the nonlinear effect, so we have to solve the system to the order $O(\nu^2)$. It is convenient to eliminate b in the original system Eq. (26). By including orders through $O(\nu^2)$, we have

$$\begin{aligned}&\partial_Z^2(\nu a_1 + \nu^2 a_2) + |\gamma|^2(\nu a_1 + \nu^2 a_2)\\ &\quad = i(\gamma\bar\nabla\gamma^* + \gamma^*\bar\nabla\gamma)\cdot\tilde\nabla(\nu a_0 + \nu^2 a_1) + \nu^2 g[i\,\partial_Z(|a_0|^2 a_0)\\ &\qquad - \gamma|b_0|^2 b_0] + \frac{\nu^2}{2}\sum_{m,n=1}^{2}(\gamma^*\,\bar\partial_{m,n}\gamma + \gamma\,\bar\partial_{m,n}\gamma^*\\ &\qquad + \bar\partial_m\gamma\,\bar\partial_n\gamma^* + \bar\partial_m\gamma^*\,\bar\partial_n\gamma)\,\tilde\partial_{m,n}a_0.\end{aligned} \tag{33}$$

We first assume $Q = 0$ and then solve the foregoing equation order by order by applying the multiscale replacement $\partial_Z \to \partial_Z + \nu\partial_{Z_1}$.

At the order $O(\nu)$, we have

$$\begin{aligned}&\partial_{Z_1}^2 a_1 + |\gamma|^2 a_1\\ &\quad = [-2i|\gamma|\partial_{Z_1}P + i(\gamma\bar\nabla\gamma^* + \gamma^*\bar\nabla\gamma)\cdot\tilde\nabla P]e^{i|\gamma|Z}.\end{aligned}$$

Removal of the secular term implies that

$$-2i|\gamma|\partial_{Z_1}P + i[(\gamma\bar\nabla\gamma^* + \gamma^*\bar\nabla\gamma)\cdot\tilde\nabla P] = 0. \tag{34}$$

It is noted that a_1 is the same as the homogeneous solution, which means $a_1 = Da_0$, where D is a constant. It is seen that a_1 does not make any contribution to next-order equations. So, we set $D = 0$ for simplicity.

The preceding equation is a transport equation. Note that

$$\nabla\mu_1 = -C\frac{\gamma\bar\nabla\gamma^* + \gamma^*\bar\nabla\gamma}{2|\gamma|}. \tag{35}$$

Then, the leading-order equation is

$$\frac{\partial P}{\partial Z_1} + \bar\nabla\tilde\mu_1\cdot\tilde\nabla P = 0, \tag{36}$$

where $\tilde\mu_1 = \frac{\mu_1}{C}$. So, $\bar\nabla\tilde\mu_1$ is the group velocity of the transport. This is similar to the homogeneous case, where the envelopes move with the group velocity. Note that the group velocity is not just the gradient but a scaled gradient. This is because the gradient is small due to the TB approximation, and we absorb it into the time scale (the propagating direction). This is similar to the simple lattice cases, where the leading-order phenomenon is governed by a transport equation [13].

We expand the equation to the next order to study the nonlinear effect. An easy way to obtain the correction to the transport equation is to insert a correction into the earlier equation, that is,

$$\frac{\partial P}{\partial Z_1} + \bar\nabla\tilde\mu_1\cdot\tilde\nabla P = \nu h, \tag{37}$$

where h is defined subsequently.

At the order $O(\nu^2)$, we have

$$\begin{aligned}\partial_Z^2 a_2 + |\gamma|^2 a_2 = &\left[-\partial_{Z_1}^2 P - 2s(\sigma)g|\gamma||P|^2 P\right]e^{i|\gamma|Z}\\ &+ \frac{1}{2}\sum_{m,n=1}^{2}(\gamma^*\,\bar\partial_{m,n}\gamma + \gamma\,\bar\partial_{m,n}\gamma^* + \bar\partial_m\gamma\,\bar\partial_n\gamma^*\\ &+ \bar\partial_m\gamma^*\,\bar\partial_n\gamma)\tilde\partial_{m,n}P\,e^{i|\gamma|Z} - 2i|\gamma|h.\end{aligned}$$

Removal of the secular terms yields that

$$\begin{aligned}&-\partial_{Z_1}^2 P - 2s(\sigma)g|\gamma||P|^2 P + \frac{1}{2}\sum_{m,n=1}^{2}(\gamma^*\,\bar\partial_{m,n}\gamma + \gamma\,\bar\partial_{m,n}\gamma^*\\ &\quad + \bar\partial_m\gamma\,\bar\partial_n\gamma^* + \bar\partial_m\gamma^*\,\bar\partial_n\gamma)\,\tilde\partial_{m,n}P - 2i|\gamma|h = 0.\end{aligned}$$

Note that

$$\partial_{Z_1}^2 P = \sum_{m,n=1}^{2}\bar\partial_m\tilde\mu_1\,\bar\partial_n\tilde\mu_1\,\tilde\partial_{m,n}P,$$

and

$$\begin{aligned}\partial_{m,n}\mu_1 = -\frac{C}{2|\gamma|}&(-2\,\bar\partial_m\tilde\mu_1\,\bar\partial_n\tilde\mu_1 + \gamma^*\,\bar\partial_{m,n}\gamma + \gamma\,\bar\partial_{m,n}\gamma^*\\ &+ \bar\partial_m\gamma\,\bar\partial_n\gamma^* + \bar\partial_m\gamma^*\,\bar\partial_n\gamma).\end{aligned} \tag{38}$$

Then, the following equation is obtained

$$\begin{aligned}&\frac{\partial P}{\partial Z_1} + \bar\nabla\tilde\mu_1\cdot\tilde\nabla P\\ &\quad + \nu\left[\frac{1}{2}\sum_{m,n=1}^{2}\bar\partial_{m,n}\tilde\mu_1\,\tilde\partial_{m,n}P + s(\sigma)g|P|^2 P\right] = 0.\end{aligned} \tag{39}$$

By introducing a moving coordinate system $\bar{\mathbf{R}} = \mathbf{R} - \bar\nabla\tilde\mu_1 Z_1$ (we drop the bar above **R**), and a new propagating

distance scale $Z_2 = \nu Z_1$, that is,

$$P(Z_1,\mathbf{R}) = P(Z_2,\mathbf{R} - \bar{\nabla}\tilde{\mu}_1 Z_1) \tag{40}$$

yields

$$i\,\partial_{Z_2} P + \frac{1}{2}\sum_{m,n=1}^{2} \bar{\partial}_{m,n}\tilde{\mu}_1\,\tilde{\partial}_{m,n} P + s(\sigma)g|P|^2 P = 0. \tag{41}$$

This is an effective NLS equation. Thus, similar to simple lattices, the governing equations are effective NLS equations when the eigenspace is 1D. Actually, this NLS equation can also be derived from a continuous multiscale expansion method (cf. Ref. [13]). Thus, we see that effective NLS equations can be derived from the unified nonlinear discrete system in honeycomb lattices when the $\mathbf{k}$ point is distinct from the Dirac points $\mathbf{K},\mathbf{K}'$. The dispersive coefficients can easily be computed via Eq. (38) in the TB limit. However, on the other hand, in a continuous multiscale expansion approach, the coefficients are not explicit, since the dispersion relation generally cannot be obtained analytically.

The original field in the lattice NLS equation has the form

$$\psi(z,\mathbf{r}) \sim P\mathbf{(}C\nu^2 z, \nu(\mathbf{r} - \bar{\nabla}\mu_1 z)\mathbf{)}e^{-i\mu_1 z},$$

where the envelope P satisfies the previous effective NLS equation Eq. (41).

Similarly, for the branch μ_2 (i.e., when $P = 0$), the governing equation is found to be

$$i\,\partial_{Z_2} Q + \frac{1}{2}\sum_{m,n=1}^{2} \bar{\partial}_{m,n}\tilde{\mu}_2\,\tilde{\partial}_{m,n} Q + s(\sigma)g|Q|^2 Q = 0. \tag{42}$$

Note that $\bar{\nabla}\tilde{\mu}_2 = -\bar{\nabla}\tilde{\mu}_1$ and $\bar{\partial}_{m,n}\tilde{\mu}_2 = -\bar{\partial}_{m,n}\tilde{\mu}_1$. So, the envelopes of the upper branch and the lower branch propagate in opposite directions and have dispersive terms with opposite signs.

As examples, we investigate the governing equations at some special points where $\bar{\nabla}\tilde{\mu}_2 = \bar{\nabla}\tilde{\mu}_1 = \mathbf{0}$ (see also Ref. [13]). The locations of these points are depicted in Fig. 2(a). We only give the Hessian matrices of the dispersion relation for the first band; the second band is the negative of the first band.

At the Γ point ($\mathbf{k} = \mathbf{0}$), $\gamma(\mathbf{0}) = \gamma^*(\mathbf{0}) = 3$. So, $\mu_1 = E_0 + c_0 - 3C$ and $\mu_2 = E_0 + c_0 + 3C$. The Hessian matrix, defined as $\bar{\mathbf{H}} = \left(\begin{smallmatrix}\bar{\partial}_{11} & \bar{\partial}_{12}\\ \bar{\partial}_{21} & \bar{\partial}_{22}\end{smallmatrix}\right)$ is

$$\bar{\mathbf{H}}\mu_1 = \frac{Cl^2}{2}\begin{pmatrix}\rho & 0\\ 0 & \frac{2\rho^2+\rho}{3}\end{pmatrix}.$$

It is seen that the Γ point on the lower branch is a minimum point, while it is the maximum point on the upper branch. So, the governing equations are

$$i\,\partial_{Z_2} P + \frac{\rho l^2}{4}\left(\partial_{XX} + \frac{2\rho+1}{3}\partial_{YY}\right) P + s(\sigma)g|P|^2 P = 0, \tag{43}$$

and

$$i\,\partial_{Z_2} Q - \frac{\rho l^2}{4}\left(\partial_{XX} + \frac{2\rho+1}{3}\partial_{YY}\right) Q + s(\sigma)g|Q|^2 Q = 0. \tag{44}$$

Thus, we replace a focusing equation with a defocusing equation.

At the M point [$\mathbf{k} = \frac{1}{2}(\mathbf{k}_1 + \mathbf{k}_2)$], the Hessian matrix is

$$\bar{\mathbf{H}}\mu_1 = C\frac{3\rho l^2}{2}\begin{pmatrix}-\frac{\rho}{2\rho-1} & 0\\ 0 & \frac{\rho}{3}\end{pmatrix}.$$

So M is a saddle point.

At the X_1 point ($\mathbf{k} = \frac{1}{2}\mathbf{k}_1$), the Hessian matrix is

$$\bar{\mathbf{H}}\mu_1 = Cl^2\begin{pmatrix}0 & \frac{\sqrt{3}\rho}{2}\\ \frac{\sqrt{3}\rho}{2} & \rho^2\end{pmatrix}.$$

X_1 is a saddle point.

At the X_2 point ($\mathbf{k} = \frac{1}{2}\mathbf{k}_2$), the Hessian matrix is

$$\bar{\mathbf{H}}\mu_1 = Cl^2\begin{pmatrix}0 & -\frac{\sqrt{3}\rho}{2}\\ -\frac{\sqrt{3}\rho}{2} & \rho^2\end{pmatrix}.$$

X_2 is a saddle point.

Therefore, at the M, X_1, and X_2 points, the governing equations are hyperbolic NLS equations.

It is noted that we obtain a focusing NLS equation at the band edge Γ point if $\sigma > 0$. It is expected that solitons will bifurcate from this point into the semi-infinite band gap. Interested readers can find experimental and numerical results in Refs. [18,19]. At the M, X_1, and X_2 points, the governing equations are hyperbolic NLS equations. Such equations have been derived in deep water waves [28]. It is not clear what interesting physical phenomenon can exist in these hyperbolic NLS equations. This deserves more study but is outside the scope of this paper.

C. Coupled NLS equations

In this section, we consider the case where the initial envelope contains both μ_1 and μ_2 components. From Sec. IV B, we know that the leading-order governing equation of each component is a transport equation. In general, each component will propagate with opposite velocities, which are $\bar{\nabla}\tilde{\mu}_1$ and $\bar{\nabla}\tilde{\mu}_2 = -\bar{\nabla}\tilde{\mu}_1$, respectively. So, there are no significant nonlinear interactions between these two components. Along each moving coordinate, we will get two decoupled transport equations to leading order. However, if the two components have nearly zero velocity [i.e., $|\bar{\nabla}\tilde{\mu}_1| \sim |\bar{\nabla}\tilde{\mu}_2| \sim O(\nu)$], they would interact with each other, and coupled NLS equations will be obtained.

Similar to the one component case, we get the envelope at the leading order:

$$a_0 = P(Z_2,\mathbf{R} - \bar{\nabla}\tilde{\mu}_1 Z_1)e^{i|\gamma|Z} + Q(Z_2,\mathbf{R} - \bar{\nabla}\tilde{\mu}_2)e^{-i|\gamma|Z}. \tag{45}$$

Introduce a unified moving coordinate system $\bar{\mathbf{R}} = \mathbf{R} - \bar{\nabla}\tilde{\mu}_1 Z_1$ (we drop the bar above $\mathbf{R}$). At the order $O(\nu^2)$, we have,

$$\partial_Z^2 a_2 + |\gamma|^2 a_2 = 2s(\sigma)g(P^2Q^* e^{3i|\gamma|Z} + Q^2P^* e^{-3i|\gamma|Z}) - 2|\gamma|\left[i\,\partial_{Z_2}P + \frac{1}{2}\sum_{m,n=1}^{2}\bar{\partial}_{m,n}\tilde{\mu}_1\,\tilde{\partial}_{m,n}P + s(\sigma)g(|P|^2+2|Q|^2)P\right]e^{i|\gamma|Z}$$
$$+2|\gamma|\left[i\,\partial_{Z_2}Q + \frac{i}{\nu}(\bar{\nabla}\tilde{\mu}_2 - \bar{\nabla}\tilde{\mu}_1)\cdot\bar{\nabla}Q + \frac{1}{2}\sum_{m,n=1}^{2}\bar{\partial}_{m,n}\tilde{\mu}_2\,\tilde{\partial}_{m,n}Q + s(\sigma)g(|Q|^2+2|P|^2)Q\right]e^{-i|\gamma|Z}.$$

Note that the terms with the phase $e^{i|\gamma|Z}$ or $e^{-i|\gamma|Z}$ are secular terms. By removing secular terms yields two equations,

$$i\,\partial_{Z_2}P + \frac{1}{2}\sum_{m,n=1}^{2}\bar{\partial}_{m,n}\tilde{\mu}_1\,\tilde{\partial}_{m,n}P + s(\sigma)g(|P|^2+2|Q|^2)P = 0,$$
$$i\,\partial_{Z_2}Q - \frac{2i}{\nu}\bar{\nabla}\tilde{\mu}_1\cdot\bar{\nabla}Q - \frac{1}{2}\sum_{m,n=1}^{2}\bar{\partial}_{m,n}\tilde{\mu}_1\,\tilde{\partial}_{m,n}Q + s(\sigma)g(|Q|^2+2|P|^2)Q = 0,$$

where we have used the fact that $\bar{\nabla}\tilde{\mu}_1 = -\bar{\nabla}\tilde{\mu}_2$ and $\bar{\partial}_{m,n}\tilde{\mu}_1 = -\bar{\partial}_{m,n}\tilde{\mu}_2$.

For instance, at the Γ point, we have the system:

$$i\,\partial_{Z_2}P + \frac{\rho l^2}{4}\left(\partial_{XX} + \frac{2\rho+1}{3}\partial_{YY}\right)P + s(\sigma)g(|P|^2+2|Q|^2)P = 0,$$
$$i\,\partial_{Z_2}Q - \frac{\rho l^2}{4}\left(\partial_{XX} + \frac{2\rho+1}{3}\partial_{YY}\right)Q + s(\sigma)g(|Q|^2+2|P|^2)Q = 0.$$

The preceding system is a defocusing-focusing coupled NLS system. When $Q = 0$, the system reduces to Eq. (43); similarly, the system reduces to Eq. (44) if $P = 0$. Thus, this is consistent with the single envelope analysis in Sec. IV B.

We note that the previous system in the 1D case was also derived in fiber communications [29]. Zakharov and Schulman found properties, which suggest the previous system is not integrable in the 1D case [30], but there still exist bright-dark soliton solutions [29]. However, there are apparently few, if any, results, known that regard the earlier 2D coupled NLS system. This system requires detailed analysis, which is outside the scope of this paper.

V. COUPLED CONTINUOUS NONLINEAR DIRAC SYSTEM

In the preceding sections, we only consider the case that the envelope is associated with one value of $\mathbf{k}$. On the other hand, sometimes input envelopes can be composed of components that belong to different values of $\mathbf{k}$ but with the same propagation constant μ. If the group velocities for different components are different, there will be no significant nonlinear interactions. However, if their group velocities happen to satisfy a further restriction so that they are nearly equal, and the values of $\mathbf{k}$ are well away from the Dirac points, usually the coupled NLS equation would be expected [e.g., one can consider envelope approximation equation Eq. (20) at two values of $\mathbf{k}$]. In this section, we consider two components associated with the two Dirac points $\mathbf{K}$ and $\mathbf{K}'$ at the same value of $\mu \sim E + c_0$. Namely, the leading-order discrete envelope would have the form

$$\psi \sim \left\{\sum_{\mathbf{v}}[a_{\mathbf{v}}\phi_1(\mathbf{r}-\mathbf{v}) + b_{\mathbf{v}}\phi_2(\mathbf{r}-\mathbf{v})]e^{i\mathbf{K}\cdot\mathbf{v}}\right\} + \left\{\sum_{\mathbf{v}}[a'_{\mathbf{v}}\phi_1(\mathbf{r}-\mathbf{v}) + b'_{\mathbf{v}}\phi_2(\mathbf{r}-\mathbf{v})]e^{i\mathbf{K}'\cdot\mathbf{v}}\right\}. \tag{46}$$

However, we will see that under evolution, a new component will be generated due to four-wave mixing [31]. So, under propagation, the envelope takes the more general form

$$\psi \sim \left\{\sum_{\mathbf{v}}[a_{\mathbf{v}}(Z)\phi_1(\mathbf{r}-\mathbf{v}) + b_{\mathbf{v}}(Z)\phi_2(\mathbf{r}-\mathbf{v})]e^{i\mathbf{K}\cdot\mathbf{v}}\right\}e^{-i(E+c_0)z} + \left\{\sum_{\mathbf{v}}[a'_{\mathbf{v}}(Z)\phi_1(\mathbf{r}-\mathbf{v}) + b'_{\mathbf{v}}(Z)\phi_2(\mathbf{r}-\mathbf{v})]e^{i\mathbf{K}'\cdot\mathbf{v}}\right\}e^{-i(E+c_0)z} + \left\{\sum_{\mathbf{v}}[u_{\mathbf{v}}(Z)\phi_1(\mathbf{r}-\mathbf{v}) + v_{\mathbf{v}}(Z)\phi_2(\mathbf{r}-\mathbf{v})]\right\}e^{-i(E+c_0)z}, \tag{47}$$

By following the same method as in the one component case in the earlier sections, we find two discrete equations,

$$\left[\varepsilon i\frac{da_{\mathbf{p}}}{dZ} + C\mathcal{L}^- b_{\mathbf{p}} + \sigma g(|a_{\mathbf{p}}|^2 + 2|a'_{\mathbf{p}}|^2)a_{\mathbf{p}}\right]e^{i\mathbf{K}\cdot\mathbf{p}} + \left[\varepsilon i\frac{da'_{\mathbf{p}}}{dZ} + C\mathcal{L}'^- b'_{\mathbf{p}} + \sigma g(|a'_{\mathbf{p}}|^2 + 2|a'_{\mathbf{p}}|^2)a'_{\mathbf{p}}\right]e^{i\mathbf{K}'\cdot\mathbf{p}} + \varepsilon i\frac{du_{\mathbf{p}}}{dZ} + C\bar{\mathcal{L}}^- v_{\mathbf{p}} + g\sigma\left[a_{\mathbf{p}}^2 a'^*_{\mathbf{p}} e^{i(2\mathbf{K}-\mathbf{K}')\cdot\mathbf{p}} + a_{\mathbf{p}}(a'^*_{\mathbf{p}})^2 e^{i(2\mathbf{K}'-\mathbf{K})\cdot\mathbf{p}}\right] = 0,$$

and

$$\left[\varepsilon i\frac{db_{\mathbf{p}}}{dZ} + C\mathcal{L}^+ a_{\mathbf{p}} + \sigma g(|b_{\mathbf{p}}|^2 + 2|b'_{\mathbf{p}}|^2)b_{\mathbf{p}}\right]e^{i\mathbf{K}\cdot\mathbf{p}} + \left[\varepsilon i\frac{db'_{\mathbf{p}}}{dZ} + C\mathcal{L}'^+ a'_{\mathbf{p}} + \sigma g(|b'_{\mathbf{p}}|^2 + 2|b_{\mathbf{p}}|^2)b'_{\mathbf{p}}\right]e^{i\mathbf{K}'\cdot\mathbf{p}} + \varepsilon i\frac{dv_{\mathbf{p}}}{dZ} + C\bar{\mathcal{L}}^+ u_{\mathbf{p}} + g\sigma\left[b_{\mathbf{p}}^2 b'^*_{\mathbf{p}} e^{i(2\mathbf{K}-\mathbf{K}')\cdot\mathbf{p}} + b_{\mathbf{p}}(b'^*_{\mathbf{p}})^2 e^{i(2\mathbf{K}'-\mathbf{K})\cdot\mathbf{p}}\right] = 0,$$

where the operator groups $(\mathcal{L}^+, \mathcal{L}^-)$ and $(\mathcal{L}'^+, \mathcal{L}'^-)$ are defined in the previous sections and are associated with $\mathbf{K}$ and $\mathbf{K}'$, respectively, while $\bar{\mathcal{L}}^+$, $\bar{\mathcal{L}}^-$ are associated with $\mathbf{k} = \mathbf{0}$.

Then, as done previously, we consider the continuous limit of the earlier systems. To introduce the envelope scale $\mathbf{R}$ and to take the maximal balance $\epsilon = C\nu = |\sigma|$ yields (note that $\mathbf{K}' = -\mathbf{K}$)

$$\left[i\partial_Z a + \frac{\sqrt{3}l}{2}(\partial_X + \zeta i\partial_Y)b + s(\sigma)g(|a|^2 + 2|a'|^2)a \right] e^{i\mathbf{K}\cdot\mathbf{r}} + \left[i\partial_Z a' + \frac{\sqrt{3}l}{2}(\partial_X - \zeta i\partial_Y)b' + s(\sigma)g(|a'|^2 + 2|a|^2)a' \right] \times e^{i\mathbf{K}'\cdot\mathbf{r}} i\partial_Z u + gs(\sigma)[a^2 a'^* e^{i(3\mathbf{K})\cdot\mathbf{r}} + a(a'^*)^2 e^{i(3\mathbf{K}')\cdot\mathbf{r}}] = 0,$$

and

$$\left[i\partial_Z b + \frac{\sqrt{3}l}{2}(-\partial_X + \zeta i\partial_Y)a + s(\sigma)g(|b|^2 + 2|b'|^2)b \right] e^{i\mathbf{K}\cdot\mathbf{r}} + \left[i\partial_Z b' + \frac{\sqrt{3}l}{2}(-\partial_X - \zeta i\partial_Y)a' + s(\sigma)g(|b'|^2 + 2|b|^2)b' \right] \times e^{i\mathbf{K}'\cdot\mathbf{r}} + i\partial_Z v + gs(\sigma)[b^2 b'^* e^{i(3\mathbf{K})\cdot\mathbf{r}} + b(b'^*)^2 e^{i(3\mathbf{K}')\cdot\mathbf{r}}] = 0.$$

In the foregoing equations, we have highly oscillatory phases $e^{i\mathbf{K}\cdot\mathbf{r}}$ and $e^{i\mathbf{K}'\cdot\mathbf{r}}$ as well as their higher harmonics. To average over the fast scale $\mathbf{r}$ implies the following coupled nonlinear Dirac system,

$$i\partial_Z u + \frac{\sqrt{3}l}{2}(\partial_X + \zeta i\partial_Y)b + s(\sigma)g(|a|^2 + 2|a'|^2)a = 0, \tag{48a}$$

$$i\partial_Z b + \frac{\sqrt{3}l}{2}(-\partial_X + \zeta i\partial_Y)a + s(\sigma)g(|b|^2 + 2|b'|^2)b = 0, \tag{48b}$$

$$i\partial_Z a' + \frac{\sqrt{3}l}{2}(\partial_X - \zeta i\partial_Y)b' + s(\sigma)g(|a'|^2 + 2|a|^2)a' = 0, \tag{48c}$$

$$i\partial_Z b' + \frac{\sqrt{3}l}{2}(-\partial_X - \zeta i\partial_Y)a' + s(\sigma)g(|b'|^2 + 2|b|^2)b' = 0, \tag{48d}$$

while the four-wave mixing components satisfy

$$i\partial_Z u + gs(\sigma)[a^2 a'^* e^{i(3\mathbf{K})\cdot\mathbf{R}/\nu} + a(a'^*)^2 e^{i(3\mathbf{K}')\cdot\mathbf{R}/\nu}] = 0, \tag{49a}$$

$$i\partial_Z v + gs(\sigma)[b^2 b'^* e^{i(3\mathbf{K})\cdot\mathbf{R}/\nu} + b(b'^*)^2 e^{i(3\mathbf{K}')\cdot\mathbf{R}/\nu}] = 0. \tag{49b}$$

Usually, the $u(Z,\mathbf{R}), v(Z,\mathbf{R})$ are zero initially, and the forcing terms have highly oscillatory phases. The resulting four-wave components are generated, but $u(Z,\mathbf{R})$ and $v(Z,\mathbf{R})$ are small compared to a, a', b, b'. Detailed analysis is omitted here. Interested readers can refer to Ref. [31].

The preceding coupled nonlinear Dirac system describes the conical diffraction phenomena in honeycomb lattices when the envelope contains two components that correspond to the two conjugate Dirac points.

VI. CONCLUSION AND DISCUSSION

In this paper, discrete and continuous Bloch-mode envelopes that propagate in generalized honeycomb lattices are studied. Similar to simple lattices, the dispersion relation plays a key role in both discrete and continuous dynamics.

In the TB limit, an analytical description of the dispersion relation can be obtained in terms of elementary functions. Unlike simple lattices [13], the dispersion relation for honeycomb lattices is not, in general, represented in a Fourier-series form. The lowest band of the dispersion relation has two branches, and there may exist Dirac points where two branches touch each other. Away from the Dirac points, the dispersion surfaces are smooth.

In general, a discrete approach is employed to find the dynamics of the wave envelope. We first derive a unified nonlinear discrete system and then consider its various continuous limits as a means to further elucidate the results. From discrete to continuous systems, the underlying mechanism and all parameters are very clear. Since honeycomb lattices contain more than one site per unit cell, the discrete approach used in this paper is different from the one that has been applied in simple lattices [13]. It is found that a unified discrete system can describe the dynamics of the wave envelope associated with any wave number $\mathbf{k}$ in the first band. When $\mathbf{k}$ is chosen to be a Dirac point, this is considered to be a nonlinear discrete Dirac system. However, it is interesting that the corresponding continuous systems for different $\mathbf{k}$ can take different forms. Near the Dirac points, the continuous governing system is a (continuous) nonlinear Dirac system. Away from Dirac points, in certain cases, the governing equations are scalar NLS equations. Coupled NLS equations can also be obtained if the input envelope contains two components that correspond to two different branches but with a small group velocity in each component. Similarly, a coupled Dirac system can be obtained when the envelopes are associated with conjugate Dirac points.

In this paper, the dynamics of the envelope associated only with the lowest band is studied. The dynamics associated with higher bands follows a similar approach. It is also noted that the dynamics of the envelope near the Dirac points changes significantly if the honeycomb lattice is deformed. The associated linear dispersion relation changes its structure, and new governing equations arise. We will report on this in a future communication.

ACKNOWLEDGMENTS

This research was partially supported by the US Air Force Office of Scientific Research, under Grant No. FA9550-09-1-0250 and by the NSF under Grant No. DMS-0905779.

APPENDIX

In this appendix, we give explicit formulas for all the parameters in our analysis when using the TB approximation. A 2D (quantum) harmonic oscillator is given by the eigenvalue problem,

$$[\nabla^2 - d_0(c^2x^2 + y^2)]\eta(\mathbf{r}) = -\epsilon\eta(\mathbf{r}),$$

where d_0 is the intensity, $c > 0$ is the anisotropy ratio, and the energy (eigenvalue) is denoted by ϵ. The associated normalized

eigenfunction is

$$\eta_{m,n}(x,y) = \sqrt{\frac{1}{2^{m+n}m!n!}}\frac{(cd_0)^{1/4}}{\pi^{1/2}}e^{-(\sqrt{d_0}/2)(cx^2+y^2)} \times H_m\big((c^2d_0)^{1/4}x\big)H_n\big(d_0^{1/4}y\big),$$

where the corresponding energy (eigenvalue) is given by $\epsilon_{m,n} = \sqrt{d_0}(c + 2mc + 1 + 2n)$.

In the TB limit, the potential has a very deep well at each site. Thus, the Bloch mode is mainly determined by the behavior of the potential near the site. In this paper, the potential we are dealing with is locally harmonic, that is,

$$V(\mathbf{r}) \approx V_0\{\hat{k}^2[c^2(x-x_0)^2 + (y-y_0)^2] - 1\}, \qquad \text{(A1)}$$

where $c^2 = \frac{(4\eta^2-1)}{3}$ and $\hat{k}^2 = \frac{9k_0^2}{4(1+2\eta)^2}$ for the potential Eq. (2).

For the low bands, $V_1(\mathbf{r})$ and $V_2(\mathbf{r})$ in Eq. (8) can usually be approximated by rapidly decaying functions. This approximation does not significantly alter the Bloch modes or the associated dispersion relation in the TB limit (via WKB theory), and it leads to detailed analytical results. This technique has been successfully implemented in simple lattices [13]. An elementary rapidly decaying function that has the asymptotic expansion Eq. (A1) is

$$V_s(\mathbf{r}) \approx -V_0\big(e^{\hat{k}^2[c^2(x-x_0)^2+(y-y_0)^2]}\big).$$

The potential Eq. (2) now is approximated by a sum of Gaussian functions. All these Gaussian functions are centered at all of the different sites (minima) and have the same local structure.

We only study the lowest band dynamics, so only the ground state of the harmonic oscillator is considered. The orbitals are then

$$\phi_1(\mathbf{r}) = \frac{(c^2\hat{k}^2V_0)^{1/4}}{\pi^{1/2}}e^{(-\hat{k}^2V_0/2)\|\mathbf{r}-A_0\|_1^2},$$

$$\phi_2(\mathbf{r}) = \frac{(c^2\hat{k}^2V_0)^{1/4}}{\pi^{1/2}}e^{(-\hat{k}^2V_0/2)\|\mathbf{r}-B_0\|_1^2},$$

and the orbital energy is

$$E = \epsilon_{0,0} - V_0 = (1+c)\hat{k}^2\sqrt{V_0} - V_0,$$

where $\|r\|_1 = \sqrt{cx^2+y^2}$ is a weighted norm and we also define $\|r\|_2 = \sqrt{c^2x^2+y^2}$.

From the symmetries, we can easily obtain that ($s = 1,2$)

$$c_0 = \lambda_{11}(\mathbf{0}) = \lambda_{22}(\mathbf{0}),$$

$$c_1 = \kappa_{12}(\mathbf{0}) = \kappa_{21}(\mathbf{0}) = \frac{1}{\rho_1}\kappa_{12}(-\mathbf{v}_s) = \frac{1}{\rho_1}\kappa_{21}(\mathbf{v}_s),$$

$$c_2 = \lambda_{12}(\mathbf{0}) = \lambda_{21}(\mathbf{0}) = \frac{1}{\rho_2}\lambda_{12}(-\mathbf{v}_s) = \frac{1}{\rho_2}\lambda_{21}(\mathbf{v}_s).$$

After some elementary but tedious calculations, we get (only leading terms are kept)

$$c_0 \approx -V_0\sum_{m=0}^{2}e^{-\hat{k}^2\|\mathbf{d}_m\|_2^2},$$

$$c_1 \approx e^{(-\hat{k}\sqrt{V_0}/4)\|\mathbf{d}_0\|_1^2},$$

$$c_2 \approx -V_0e^{-(\hat{k}\sqrt{V_0}/4)\|\mathbf{d}_0\|_1^2}e^{(-\hat{k}^2/4)\|\mathbf{d}_0\|_2^2},$$

$$\rho_1 \approx e^{(-\hat{k}\sqrt{V_0}/4)(\|\mathbf{d}_1\|_1^2-\|\mathbf{d}_0\|_1^2)},$$

$$\rho_2 \approx e^{(-\hat{k}\sqrt{V_0}/4)(\|\mathbf{d}_1\|_1^2-\|\mathbf{d}_0\|_1^2)}e^{(-\hat{k}^2/4)(\|\mathbf{d}_1\|_2^2-\|\mathbf{d}_0\|_2^2)}.$$

If we only keep the leading-order terms under the limit $V_0 \gg 1$, we get the key parameters we used in this paper:

$$C = V_0e^{(-\hat{k}\sqrt{V_0}/4)\|\mathbf{d}_0\|_1^2}\left(e^{(-\hat{k}^2/4)\|\mathbf{d}_0\|_2^2} - \sum_{m=0}^{2}e^{-\hat{k}^2\|\mathbf{d}_m\|_2^2}\right),$$

$$\rho = e^{(-\hat{k}\sqrt{V_0}/4)(\|\mathbf{d}_1\|_1^2-\|\mathbf{d}_0\|_1^2)}\frac{e^{(-\hat{k}^2/4)\|\mathbf{d}_1\|_2^2} - \sum_{s=0}^{2}e^{-\hat{k}^2\|\mathbf{d}_s\|_2^2}}{e^{(-\hat{k}^2/4)\|\mathbf{d}_0\|_2^2} - \sum_{s=0}^{2}e^{-\hat{k}^2\|\mathbf{d}_s\|_2^2}},$$

$$g = \frac{\hat{k}\sqrt{cV_0}}{2\pi}.$$

For the undeformed lattice ($\eta = 1$), $\rho = 1$ and $C \approx 0.3V_0e^{-2\sqrt{V_0}\pi^2/9k_0}$.

[1] D. Christodoulides and R. Joseph, Opt. Lett. **13**, 794 (1988).
[2] H. Eisenberg, Y. Silberberg, R. Morandotti, A. Boyd, and J. Aitchison, Phys. Rev. Lett. **81**, 3383 (1998).
[3] J. W. Fleischer, T. Carmon, M. Segev, N. K. Efremidis, and D. N. Christodoulides, Phys. Rev. Lett. **90**, 023902 (2003).
[4] J. W. Fleischer, M. Segev, N. K. Efremidis, and D. N. Christodoulides, Nature (London) **422**, 147 (2003).
[5] O. Morsch and M. Oberthaler, Rev. Mod. Phys. **78**, 179 (2006).
[6] J. K. Yang, I. Makasyuk, A. Bezryadina, and Z. Chen, Opt. Lett. **29**, 1662 (2004).
[7] D. N. Neshev, T. J. Alexander, E. A. Ostrovskaya, Y. S. Kivshar, I. Martin, H. Makasyuk, and Z. G. Chen, Phys. Rev. Lett. **92**, 123903 (2004).
[8] X. Wang, Z. Chen, J. Wang, and J. Yang, Phys. Rev. Lett. **99**, 243901 (2007).
[9] Z. Shi and J. Yang, Phys. Rev. E **75**, 056602 (2007).
[10] B. Ilan and M. I. Weinstein, SIAM J. Multiscale Model. Simul. **8**, 1055 (2010).
[11] M. J. Ablowitz, B. Ilan, E. Schonbrun, and R. Piestun, Phys. Rev. E **74**, 035601(R) (2006).
[12] B. Freedman, G. Bartal, M. Segev, R. Lifshitz, D. N. Christodoulides, and J. W. Fleischer, Nature (London) **440**, 1166 (2006).
[13] M. J. Ablowitz and Y. Zhu (unpublished).
[14] M. V. Berry and M. R. Jeffrey, Prog. Opt. **50**, 13 (2007).
[15] A. K. Geim and K. S. Novoselov, Nat. Mater. **6**, 183 (2007).
[16] M. Ablowitz, S. Nixon, and Y. Zhu, Phys. Rev. A **79**, 053830 (2009).
[17] L. H. Haddad and L. C. Carr, Physica D **238**, 1413 (2009).
[18] O. Peleg, G. Bartal, B. Freedman, O. Manela, M. Segev, and D. N. Christodoulides, Phys. Rev. Lett. **98**, 103901 (2007).
[19] P. G. Kevrekidis, B. A. Malomed, and Y. B. Gaididei, Phys. Rev. E **66**, 016609 (2002).
[20] C. R. Rosberg, D. N. Neshev, A. A. Sukhorukov, W. Krolikowski, and Y. S. Kivshar, Opt. Lett. **32**, 397 (2007).
[21] O. Bahat-Treidel, O. Peleg, and M. Segev, Opt. Lett. **33**, 2251 (2008).

[22] P. G. Kevrekidis, K. O. Rasmussen, and A. R. Bishop, Int. J. Mod. Phys. B **15**, 2833 (2001).
[23] G. L. Alfimov, P. G. Kevrekidis, V. V. Konotop, and M. Salerno, Phys. Rev. E **66**, 046608 (2002).
[24] J. Callaway, *Quantum Theory of the Solid State*, 2nd ed. (Academic, New York, 1991).
[25] G. H. Wannier, Phys. Rev. **52**, 191 (1937).
[26] F. Odeh and J. B. Keller, J. Math. Phys. **5**, 1499 (1964).
[27] A. S. Davydov, Usp. Fiz. Nauk **82**, 393 (1964) [Sov. Phys. Usp. **7**, 145 (1964)].
[28] V. E. Zakharov, J. Appl. Mech. Tech. Phys. **2**, 190 (1968).
[29] V. V. Afanasyev, Y. S. Kivshar, V. V. Konotop, and V. N. Serkin, Opt. Lett. **14**, 805 (1989).
[30] V. E. Zakharov and E. I. Schulman, Physica D **4**, 270 (1982).
[31] M. J. Ablowitz, G. Biondini, S. Chakravarty, R. B. Jenkins, and J. R. Sauer, Opt. Lett. **21**, 1646 (1996).